

VU Research Portal

Ancient volcanism on the Moon

Snape, Joshua F.; Curran, Natalie M.; Whitehouse, Martin J.; Nemchin, Alexander A.; Joy, Katherine H.; Hopkinson, Tom; Anand, Mahesh; Bellucci, Jeremy J.; Kenny, Gavin G.

published in

Earth and Planetary Science Letters
2018

DOI (link to publisher)

[10.1016/j.epsl.2018.08.035](https://doi.org/10.1016/j.epsl.2018.08.035)

document version

Peer reviewed version

document license

CC BY-NC-ND

[Link to publication in VU Research Portal](#)

citation for published version (APA)

Snape, J. F., Curran, N. M., Whitehouse, M. J., Nemchin, A. A., Joy, K. H., Hopkinson, T., Anand, M., Bellucci, J. J., & Kenny, G. G. (2018). Ancient volcanism on the Moon: Insights from Pb isotopes in the MIL 13317 and Kalahari 009 lunar meteorites. *Earth and Planetary Science Letters*, 502, 84-95.
<https://doi.org/10.1016/j.epsl.2018.08.035>

General rights

Copyright and moral rights for the publications made accessible in the public portal are retained by the authors and/or other copyright owners and it is a condition of accessing publications that users recognise and abide by the legal requirements associated with these rights.

- Users may download and print one copy of any publication from the public portal for the purpose of private study or research.
- You may not further distribute the material or use it for any profit-making activity or commercial gain
- You may freely distribute the URL identifying the publication in the public portal ?

Take down policy

If you believe that this document breaches copyright please contact us providing details, and we will remove access to the work immediately and investigate your claim.

E-mail address:

vuresearchportal.ub@vu.nl

Ancient volcanism on the Moon: Insights from Pb isotopes in the MIL 13317 and Kalahari 009 lunar meteorites

Authors: Joshua F. Snape^{1,2*}, Natalie M. Curran^{3,4}, Martin J. Whitehouse¹, Alexander A. Nemchin^{1,5}, Katherine H. Joy³, Tom Hopkinson⁶, Mahesh Anand^{6,7}, Jeremy J. Bellucci¹, Gavin G. Kenny¹

Affiliations:

¹ Department of Geosciences, Swedish Museum of Natural History, SE-104 05 Stockholm, Sweden

² Department of Earth Sciences, Faculty of Science, Vrije Universiteit Amsterdam, De Boelelaan 1085, 1081 HV Amsterdam, The Netherlands

³ School of Earth and Environmental Sciences (SEES), University of Manchester, Oxford Road, Manchester M13 9PL, UK

⁴ NASA Goddard Space Flight Center, 8800 Greenbelt Road, Greenbelt, MD 20771, USA

⁵ Department of Applied Geology, Curtin University, Perth, WA 6845, Australia

⁶ School of Physical Science, The Open University, Milton Keynes, MK7 6AA, UK

⁷ Department of Earth Sciences, The Natural History Museum, London, SW7 5BD, UK

*Corresponding author (j.f.snape@vu.nl)

Abstract

Lunar meteorites provide a potential opportunity to expand the study of ancient (> 4000 Ma) basaltic volcanism on the Moon, of which there are only a few examples in the Apollo sample collection. Secondary Ion Mass Spectrometry (SIMS) was used to determine the Pb isotopic compositions of multiple mineral phases (Ca-phosphates, baddeleyite K-feldspar, K-rich glass and plagioclase) in two lunar meteorites, Miller Range (MIL) 13317 and Kalahari (Kal) 009. These data were used to calculate crystallisation ages of 4332 ± 2 Ma (95% confidence level) for basaltic clasts in MIL 13317, and 4369 ± 7 Ma (95% confidence level) for the monomict basaltic breccia Kal 009. From the analyses of the MIL 13317 basaltic clasts, it was possible to determine an initial Pb isotopic composition of the protolith from which the clasts originated, and infer a $^{238}\text{U}/^{204}\text{Pb}$ ratio (μ -value) of 850 ± 130 (2σ

uncertainty) for the magmatic source of this basalt. This is lower than μ -values determined previously for KREEP-rich (an acronym for K, Rare Earth Elements and P) basalts, although analyses of other lithological components in the meteorite suggest the presence of a KREEP component in the regolith from which the breccia was formed and, therefore, a more probable origin for the meteorite on the lunar nearside. It was not possible to determine a similar initial Pb isotopic composition from the Kal 009 data, but previous studies of the meteorite have highlighted the very low concentrations of incompatible trace elements and proposed an origin on the farside of the Moon. Taken together, the data from these two meteorites provide more compelling evidence for widespread ancient volcanism on the Moon. Furthermore, the compositional differences between the basaltic materials in the meteorites provide evidence that this volcanism was not an isolated or localised occurrence, but happened in multiple locations on the Moon and at distinct times. In light of previous studies into early lunar magmatic evolution, these data also imply that basaltic volcanism commenced almost immediately after Lunar Magma Ocean (LMO) crystallisation, as defined by Nd, Hf and Pb model ages at about 4370 Ma.

1. Introduction

Lunar basalts collected during the Apollo and Luna missions have crystallisation ages ranging from approximately 4300-3100 Ma, but the vast majority comprise the mare basalts collected during the Apollo 11, 12, 15 and 17 missions, which have been dated to between 3800-3100 Ma (Nyquist and Shih 1992; for a more recent summary of lunar basalt ages see also Joy and Arai 2013). The crystallisation ages of the Apollo basalt samples have been combined with crater counting statistics for exposed mare basalt units across the lunar surface, obtained from orbital imagery, indicating that the exposed basalt flows were emplaced between 4000-1200 Ma, with a peak in basalt eruption between approximately 3700-3300 Ma (Hiesinger et al. 2003; 2010). Remote sensing evidence for ancient (>4000 Ma) mare volcanism was recognised by Schultz and Spudis (1979; 1983), who interpreted “dark-haloed” impact craters as instances where basaltic flows had been buried by the ejecta deposits from large impact craters, and then subsequently re-exposed by smaller impacts. These deposits of buried basaltic flows were designated the term “cryptomare” (Head and Wilson 1992). More recent remote sensing analyses of cryptomare deposits indicate a range of compositions consistent with the exposed mare basalts (Whitten and Head 2015a), as well as a geographical distribution of ancient lunar volcanism that mirrors the nearside-farside asymmetry of the younger basaltic flows (Whitten and Head 2015b).

Using the compositional classification scheme proposed by Neal and Taylor (1992), the lunar mare basalts can be defined first by their bulk TiO_2 content (where: > 6 wt% = high-Ti; 1-6 wt% = low-Ti; <1 wt% = very low-Ti [VLT]), then by Al_2O_3 content (>11 wt% = high-Al; < 11 wt% = low-Al) and finally by K content (> 2000 ppm = high-K; <2000 ppm = low-K). Sample-based evidence for ancient lunar volcanism was first identified in a number of Apollo 14 breccias, which were found to contain low-Ti, high-Al basaltic clasts with high concentrations of incompatible trace elements (ITEs), some of which are potentially as old as 4300-4200 Ma (Taylor et al. 1983; Shih et al. 1986; 1987; Dasch et al. 1987; Nyquist and Shih 1992; Neal and Kramer 2006). This has since been supplemented by evidence from lunar meteorites. Firstly, in the basaltic breccia meteorite Kalahari (Kal) 009, with U-Pb dating of Ca-phosphate grains and Lu-Hf analyses of mineral separates indicating crystallisation

ages of 4350 ± 150 Ma and 4286 ± 95 Ma, respectively (Terada et al. 2007; Sokol et al. 2008). Subsequent investigation of the same meteorite by Shih et al. (2008) yielded a Sm-Nd isochron age of 4300 ± 50 Ma. These ages, combined with minor and trace element analyses of the meteorite, were interpreted as evidence that the basaltic material in Kal 009 was sourced from cryptomare basalt that (in contrast to the Apollo 14 basaltic clasts) had a VLT, high-Al composition and very low-ITE concentrations. More recently, U-Pb analyses of baddeleyite, Ca-phosphate and tranquillityite in the basaltic-bearing anorthositic breccia Miller Range (MIL) 13317 provided $^{207}\text{Pb}/^{206}\text{Pb}$ ages that were interpreted as evidence for two mare basalt lithologies with primary crystallisation ages of 4270 ± 24 Ma and 4352 ± 9 Ma (Shaulis et al. 2016). The presence of zirconium-rich phases, such as those identified in MIL 13317, is typically associated with evolved lunar lithologies that are more ITE-rich than the Kal 009 basalt. Similarly, modelling of the MIL 13317 bulk rock composition (Zeigler and Korotev 2016) suggests that the breccia matrix contains a mixture of mare basalt and KREEP-rich lithologies (a geochemical signature defined by elevated concentrations of K, Rare Earth Elements, and P).

In this study, the Pb isotopic compositions of multiple phases in the MIL 13317 basaltic clasts have been determined with Secondary Ion Mass Spectrometry (SIMS). This approach follows the one described by Snape et al. (2016; 2018), which demonstrated the potential for Pb isotopic analyses of lunar basalts to provide precise crystallisation ages, as well as estimates for the Pb isotopic composition of the basalts at the time of crystallisation (herein referred to as the initial Pb isotopic composition). The analytical approach outlined by Snape et al. (2016) was initially applied to mare basalt samples, but it has since been successfully used in non-basalt samples including the Apollo 16 impact melt breccia, 66095, and clasts of evolved lithologies in two Apollo 14 breccias (Snape et al. 2017; Nemchin et al. 2017). By applying the same method to basaltic clasts in the MIL 13317 breccia, this study aims to test the potential link between $^{207}\text{Pb}/^{206}\text{Pb}$ ages of minerals in the meteorite matrix with the clasts, and determine the initial Pb isotopic composition for some of the oldest identified lunar basalts. Additionally, new SIMS analyses have been made of phosphates in the Kal 009

meteorite in order to more precisely constrain its age and enable a more insightful comparison with the ages of the MIL 13317 basalt clasts.

2. Methods

2.1. Sample descriptions

2.1.1. MIL 13317

MIL 13317 was found in 2013 by the Antarctic Search for Meteorites Programme (ANSMET). Despite initial classification as an anorthositic breccia (Satterwhite and Righter 2015), more detailed investigations demonstrated that the breccia has a mafic composition more consistent with it having a basaltic origin (Korotev and Irving 2016; Zeigler and Korotev 2016; Curran et al. 2016). Pyroxene compositions determined by Curran et al. (2016) are consistent with the basaltic clasts being fragments of VLT to low-Ti (where $\text{TiO}_2 = 1\text{-}6\text{ wt\%}$; Neal and Taylor 1992) mare basalts.

The Pb isotopic compositions were determined for accessory phases in five clasts, previously identified by Curran et al. (2016), and indicated in Fig. 1a (see also supplementary Fig. A.1). Three of these clasts were classified as fragments of basalt (Clasts 1, 4 and 10; Figs. 1b,c,e), and are composed primarily of subophitic intergrowths of pyroxene and plagioclase (with typical grain sizes of $\sim 100\text{-}500\text{ }\mu\text{m}$), with smaller (typically $\sim 200\times 30\text{ }\mu\text{m}$) laths of a silica polymorph. Interstitial sites between these phases are occupied by areas of late-stage mesostasis, containing K-feldspar, K-rich glass and phosphates, which were the primary targets for the SIMS analyses. A fourth clast ($600\times 350\text{ }\mu\text{m}$) is a fragment of apparently more evolved granitic material dominated by K-rich glass and silica (Clast 22; Fig. 1d), but could potentially be a particularly large fragment of mesostasis from the same basaltic material as the first three clasts. The final clast analysed (Clast 2; Fig. 1e) was described by Curran et al. (2016) as a basaltic crystalline impact melt clast and lies adjacent to Clast 10. Despite containing a similar range of phases to the basalt clasts (i.e. pyroxene, plagioclase, silica and mesostasis), the impact melt clast is somewhat finer grained (typical grain sizes of $\sim 50\text{-}200\text{ }\mu\text{m}$) than the basalts and has more K-rich plagioclase compositions. Additionally, a number of analyses were made in mineral fragments within the breccia matrix.

2.1.2. Kalahari 009

The Kal 008 and 009 meteorites were recovered in Botswana in 1999 (Russell et al. 2005). Although the two stones are paired, they are very different, with Kal 008 being classified as an anorthositic breccia, while Kal 009 is a brecciated VLT mare basalt (a detailed discussion of the geochemistry and petrology for both stones is provided by Sokol et al. 2008). Despite the VLT bulk composition and low bulk rock ITE abundances of the sample compared with most Apollo basalts, mineral chemistry data from the major silicate phases reported by Sokol et al. (2008) are consistent with VLT and low-Ti basalts, including those collected at both the Apollo 12, 15, 17 and Luna 24 landing sites (Figs. A.2. and A.3.). The meteorite is generally divided into areas of where the original igneous texture has been preserved and those that are more pervasively fractured (Fig. 2a). The Kal 009 basalt lacks most of the late-stage phases (e.g. K-feldspar, K-rich glass, zircon; Sokol et al. 2008) that have been successfully used to construct Pb-Pb isochrons in other lunar basalts (Snape et al. 2016; 2018), however, several small (10-30 μm) phosphate grains are present in the more brecciated regions of the meteorite, including those analysed previously by Terada et al. (2007). The meteorite also displays clear evidence of terrestrial weathering, with Ca-carbonate filling many of the fractures and veins in the samples (Fig. 2b-c). Sokol et al. (2008) also reported the presence of what they describe as K-rich “cauliflower-like structures”, which they also attribute to terrestrial weathering (Figs. 2a-e).

2.2. Analytical protocol

The MIL 13317,7 thin section was provided by NASA’s Meteorite Working Group. The two sections of Kal 009 analysed in this study are the same as those previously studied by Terada et al. (2007) and Sokol et al. (2008). All of the sections were cleaned with ethanol before being carbon coated. Back Scattered Electron (BSE) images and X-ray elemental maps of each section were acquired using a Quanta 650 FEGSEM and accompanying Oxford Instruments Energy Dispersive Spectroscopy (EDS) detector at Stockholm University, operating with an accelerating voltage of 20 kV at a working distance of 10 mm.

Following the SEM documentation and prior to the SIMS analyses, the samples were cleaned with a fine (1 μm) diamond paste and ethanol to remove the carbon coating before adding a 30 nm gold coating. The Pb isotopic compositions of the phases were determined during three analytical sessions using a CAMECA IMS 1280 ion microprobe at the NordSIMS facility in the Swedish Museum of Natural History, Stockholm, using a methodology similar to that outlined in previous studies (Whitehouse et al. 2005; Bellucci et al. 2015). Apertures in the primary column were used to generate a slightly elliptical O_2^- sample probe with dimensions appropriate to the target. The smaller phases (including K-rich glass, K-feldspar and phosphates) were analysed using either $\sim 5\ \mu\text{m}$ or $\sim 10\ \mu\text{m}$ spots (beam current typically 0.3-0.5 nA or 1-2 nA, respectively), while several plagioclase grains in the MIL 13317 clasts and the Ca- and K-rich material in the fractures of Kal 009 were analysed with a $\sim 30\ \mu\text{m}$ spot (13-16 nA). Prior to each measurement, an area of 20-35 μm around the spot location was rastered for 240 seconds in order to remove the gold coating and minimise possible surface contamination. The instrument was operated in high-transmission mode, corresponding to a transfer magnification of 160 \times . In this mode, the field aperture size was chosen to limit the field of view on the sample surface (i.e. the area from which ions will be admitted to the mass spectrometer) to be bigger than the unrastered spot but smaller than the rastered beam, further minimising the possibility of surface contamination. The mass spectrometer was operated with a nominal mass resolution of 4860 ($M/\Delta M$), sufficient to resolve Pb from known molecular interferences. A Nuclear Magnetic Resonance (NMR) field sensor regulated the stability of the magnetic field to high precision. For analytical sessions 1, 3 and 4 (Table B.1) the Pb isotopes were measured simultaneously in multi-collector mode using four low-noise (<0.006 counts per second) ion counting electron multipliers (Hamamatsu 416) with electronically-gated deadtimes of 65 ns. Background counts for each channel were measured at regular intervals during each session. The average background values are reported in Table B.2. Individual analyses were filtered out of the final dataset if the count rates for any masses were lower than 3 \times the average background count rates during that session.

Analyses of the MPI-DING glass reference material, GOR132, and the USGS basaltic glass reference material, BCR-2G, were used to generate a correction factor to account for mass fractionation and

detector relative gain calibration in the unknown analyses, assuming the values of Jochum et al. (2005) and Woodhead and Hergt (2000). The correction procedure involved dividing each of the “accepted” isotope ratios for GOR132 and BCR2-G (determined independently using MC-ICP-MS and TIMS analyses, respectively; Jochum et al. 2005; Woodhead and Hergt 2000), by the corresponding average of each ratio obtained from all standards in a given session in order to obtain a ratio-specific correction factor that incorporates both mass bias (a few parts per thousand at Pb mass; Shimizu and Hart 1982) and inter-detector (a few percent) gain (Table B.3.). Isotope ratios of unknown samples were then corrected by multiplying by these factors. Within uncertainty limits, no systematic drift was observed in the GOR132 and BCR2-G measurements during a given analytical session. The reproducibility of the GOR132 measurements (for the MIL 13317 analyses) was as follows: $^{208}\text{Pb}/^{206}\text{Pb} = 0.30\%$; $^{207}\text{Pb}/^{206}\text{Pb} = 0.28\%$; $^{208}\text{Pb}/^{204}\text{Pb} = 0.94\%$; $^{207}\text{Pb}/^{204}\text{Pb} = 0.74\%$; $^{206}\text{Pb}/^{204}\text{Pb} = 0.89\%$ (reported as 2σ standard deviations from the session average values for each ratio). The equivalent values for the BCR-2G measurements (two sessions for the Kal 009 analyses) were: $^{208}\text{Pb}/^{206}\text{Pb} = 0.77\%$ and 0.26% ; $^{207}\text{Pb}/^{206}\text{Pb} = 1.00\%$ and 0.22% ; $^{208}\text{Pb}/^{204}\text{Pb} = 1.19\%$ and 0.73% ; $^{207}\text{Pb}/^{204}\text{Pb} = 1.24\%$ and 0.80% ; $^{206}\text{Pb}/^{204}\text{Pb} = 0.68\%$ and 0.80% . The standard deviations obtained from the GOR132 and BCR2-G analyses, the published uncertainties on the accepted values (Woodhead and Hergt 2000; Jochum et al. 2005) and the uncertainties on each unknown analysis were propagated to determine the overall uncertainties of gain and mass bias corrected data, which are stated in Table B.1.

Data were processed using in-house SIMS data reduction spreadsheets and the Excel add-in Isoplot (version 4.15; Ludwig 2008). Calculated ages are quoted at the 95% confidence level in the following discussion.

2.3. Data reduction

The datasets were processed using the approach outlined in Snape et al. (2016), with the assumption that they represent a mixture between three main components: (1) initial Pb present in the basaltic melt when it crystallised; (2) radiogenic Pb formed by the decay of U in the basalt after crystallisation; and (3) terrestrial contamination. On a plot of $^{207}\text{Pb}/^{206}\text{Pb}$ and $^{204}\text{Pb}/^{206}\text{Pb}$, this three-component mixture

will define a triangular area (Fig. 3), with the initial Pb (or at least the lowest estimate for the initial Pb available from the data) corresponding to the highest $^{207}\text{Pb}/^{206}\text{Pb}$ values, the radiogenic Pb where $^{204}\text{Pb}/^{206}\text{Pb} = 0$, and (Fig. 3), and the terrestrial contaminant corresponding to the highest $^{204}\text{Pb}/^{206}\text{Pb}$ values. Based on this assumption, the isochron for a given basaltic sample or clast is defined by the left side of this triangle, which can be determined by iteratively filtering the data to yield the steepest statistically significant weighted regression (i.e. $\text{MSWD} < 2$; probability > 0.1). For the MIL 13317 basaltic clasts, data interpreted as showing signs of terrestrial contamination, according to the three-component mixing assumption, all have high weighted residual values (>1.5) when included in the Isoplot regression calculation.

In the case of Kal 009, the lack of different late-stage mineral phases in the analysed thin sections precludes the construction of an equivalent Pb-Pb isochron representing the crystallisation age of the basalt. Nonetheless, a weighted average $^{207}\text{Pb}/^{206}\text{Pb}$ age was determined from analyses of Ca-phosphates in the sample assuming that the Pb isotopic compositions analysed in these phases primarily represent the bottom left corner of the triangle described above (i.e. radiogenic Pb formed by the decay of U in the basalt after crystallisation), and that any ^{204}Pb present is due to terrestrial contamination, which was corrected for using the modern day terrestrial Pb model values of Stacey and Kramers (1975). This is the same approach that has been demonstrated in numerous previous studies on a variety of different samples (e.g. Terada and Sano 2003; Terada et al. 2007; Nemchin et al. 2009; Thiessen et al. 2017).

3. Results

3.1. MIL 13317

The data from each clast in MIL 13317 (Table B.1.) were first filtered following the procedure outlined above and described previously by Snape et al. (2016; 2017), in order to remove analyses clearly affected by terrestrial contamination, potentially introduced by weathering prior to collection of the meteorite, or during sample preparation and polishing (Fig. 3; Fig. A.4.; Table B.1). Notably, the effects of such contamination are relatively minor, even when compared with some Apollo basalts

(Snape et al. 2016). When plotted on axes of $^{207}\text{Pb}/^{206}\text{Pb}$ versus $^{204}\text{Pb}/^{206}\text{Pb}$, the effect of terrestrial contamination is apparent, as it results in analyses lying further to the right of the more radiogenic uncontaminated lunar compositions (Fig. 3; Fig. A.4.; Table B.1).

The data from the three basaltic clasts (Clasts 1, 4 and 10) and the granitic clast (Clast 22) form trends equating to Pb-Pb isochron dates of approximately 4330 Ma (Table 1; Fig. 4). The data from these individual clast isochrons can also be combined to form a single statistically valid (MSWD = 1.19; P = 0.17) isochron, equating to a date of 4332 ± 2 Ma (Table 1; Fig. 4f). In each of the three basaltic clasts there also appears to be a single outlier (two analyses in Clast 4 were repeat measurements of the same point to confirm the compositions; Table B.1) lying slightly above and left of the isochrons (Figs. 4a-c). These outliers were excluded from the isochrons and the dates quoted here. Nonetheless, the most radiogenic compositions determined in each of the basaltic clasts have sufficiently low $^{204}\text{Pb}/^{206}\text{Pb}$ ratios that including these outliers in the isochrons would not affect the isochron ages beyond the level of uncertainty. An alternative isochron, incorporating these outliers, and equating to a date of 4330 ± 3 Ma (MSWD = 1.05; P = 0.40) is presented in supplementary Fig. A.5 (see also Table B.1). A significantly younger Pb-Pb isochron date of 4270 ± 10 Ma is obtained for the basaltic impact melt clast (Table 1; Fig. 4e).

In addition to having indistinguishable Pb-Pb isochron dates, the least radiogenic Pb isotopic compositions measured in the three basaltic clasts are also similar (Table 1). As such, x-y weighted average values were calculated using four plagioclase analyses (one from Clast 1 and two from both Clast 4 and Clast 10), yielding a Pb isotopic composition of $^{204}\text{Pb}/^{206}\text{Pb} = 0.0251 \pm 0.0023$, $^{207}\text{Pb}/^{206}\text{Pb} = 1.596 \pm 0.030$ and $^{208}\text{Pb}/^{206}\text{Pb} = 1.339 \pm 0.026$ (2σ) (Table 1; Fig. 4f). This is interpreted as providing the best estimate (i.e. lowest possible value) for the initial Pb isotopic composition of the basaltic protolith from which the clasts originated.

A majority of the matrix mineral grains analysed (K-rich glass and mesostasis areas) have compositions consistent with being derived from the same basaltic precursor, albeit with varying degrees of terrestrial contamination (Fig. 5; Table B.1). Two analyses of K-rich glass in the matrix

have significantly more radiogenic compositions, plotting above and left of the combined isochron for the basalt clasts (Fig. 5a).

Plotting the $^{208}\text{Pb}/^{206}\text{Pb}$ ratios against $^{204}\text{Pb}/^{206}\text{Pb}$ and $^{207}\text{Pb}/^{206}\text{Pb}$, the filtered datasets for each of the basalt clasts lie on a plane in the 3D coordinate space. Although the initial Pb compositions converge at a $^{208}\text{Pb}/^{206}\text{Pb}$ ratio of 1.344 ± 0.024 , the measurements of phases containing more Pb from *in situ* radiogenic decay spread out, such that the purely radiogenic endmember compositions would be between $^{208}\text{Pb}/^{206}\text{Pb} \sim 0.4\text{--}5.1$ (Figs. 6a-d). This range in radiogenic $^{208}\text{Pb}/^{206}\text{Pb}$ ratios is interpreted as variability in $^{232}\text{Th}/^{238}\text{U}$ ratios between different mineral phases within the samples. Taking the crystallisation age of the basalt clasts into account, these $^{208}\text{Pb}/^{206}\text{Pb}$ values would correspond to $^{232}\text{Th}/^{238}\text{U}$ ratios of between $\sim 0.0\text{--}4.8$. A similar relationship is observed for the $^{208}\text{Pb}/^{206}\text{Pb}$, $^{204}\text{Pb}/^{206}\text{Pb}$ and $^{207}\text{Pb}/^{206}\text{Pb}$ ratios in impact melt Clast 2, with the range of radiogenic $^{208}\text{Pb}/^{206}\text{Pb}$ ratios (between $\sim 0.4\text{--}7.0$; Fig. 6e) equating to $^{232}\text{Th}/^{238}\text{U}$ ratios of between $\sim 0.1\text{--}6.7$.

3.2. Kalahari 009

The five phosphates analysed in the Kal 009 thin sections with the most radiogenic compositions (i.e. the lowest $^{204}\text{Pb}/^{206}\text{Pb}$ and $^{207}\text{Pb}/^{206}\text{Pb}$ ratios) yield a combined weighted average $^{207}\text{Pb}/^{206}\text{Pb}$ date of 4369 ± 7 Ma (MSWD = 0.57; P = 0.68; Fig. 7), when corrected for the presence of terrestrial contamination (assuming the modern day terrestrial Pb model values of Stacey and Kramers 1975). Several measurements were also made of the Ca- and K-rich material filling fractures in the sections and the K-rich ‘cauliflower-like’ structures identified by Sokol et al. (2008). The Pb isotopic compositions from these measurements plot in the same vicinity as the Stacey and Kramers (1975) model composition for modern terrestrial Pb. As such, the values from these Ca- and K-rich phases can be combined with all but one of the phosphate analyses (phosphate analysis “@3” in Section 2; Table B1), to construct a weighted regression line (independent of the model value from Stacey and Kramers 1975), which would also equate to a date of 4369 ± 7 Ma (MSWD = 0.41; P = 0.91; Fig. 8). This weighted regression line would essentially represent the bottom edge of the three-component

mixing triangles described in the previous section (see also Fig. 3), with the outlier phosphate datum lying within the mixing triangle for the Kal 009 sample.

4. Discussion

4.1. Interpretation of MIL 13317 isochrons

Given the crystalline nature of the MIL 13317 basalt clasts and the similarity in the Pb isotopic compositions, the isochron dates are interpreted as representing the age of crystallisation for the original igneous basalt protolith from which Clasts 1, 4, 10 and 22 were sourced. This 4332 ± 2 Ma crystallisation age is slightly younger than the $^{207}\text{Pb}/^{206}\text{Pb}$ dates (4352 ± 9 Ma) determined for phosphate and tranquillityite grains in the meteorite by Shaulis et al. (2016). This either suggests that the clasts originated from a separate igneous precursor to that of the previously analysed grains, or that there is an inaccuracy with either the $^{207}\text{Pb}/^{206}\text{Pb}$ dates or those derived from the Pb-Pb isochrons that is not reflected in the stated uncertainties. One likely source of such inaccuracy in the $^{207}\text{Pb}/^{206}\text{Pb}$ dates would be an inappropriate correction of the $^{207}\text{Pb}/^{206}\text{Pb}$ ratios for the presence of terrestrial contamination if the analyses actually sampled small amounts of a lunar initial Pb component. Given the very radiogenic nature of lunar Pb isotopic compositions (Snape et al. 2016) when compared with those of terrestrial systems (Stacey and Kramers 1975; Zartman and Doe 1981; Kramers and Tolstikhin 1997), correction of data with lunar Pb isotopic compositions will result in lower $^{207}\text{Pb}/^{206}\text{Pb}$ ratios and younger dates than if the data are corrected with terrestrial compositions (or if they are not corrected at all). The Pb-Pb isochron approach used here to determine the crystallisation ages of the MIL 13317 clasts bypasses the need for a correction with an assumed composition by measuring multiple phases that include varying proportions of Pb generated by radiogenic decay of U and Th since the rock first crystallised and lunar initial Pb. Therefore, it is possible that the grains analysed by Shaulis et al. (2016) may in fact be slightly younger than the reported $^{207}\text{Pb}/^{206}\text{Pb}$ dates and closer to the crystallisation age inferred for the basaltic clasts based on the Pb-Pb isochrons. Despite this caveat regarding the $^{207}\text{Pb}/^{206}\text{Pb}$ dates, analyses of matrix baddeleyite grain by Curran et al. (in review) made on the same CAMECA IMS 1280 instrument with a similar methodology to this study, yield compositions lying just above the combined basaltic clast isochron (Fig. 5b), indicating

that there may indeed be a separate slightly older igneous precursor that has been sampled by the meteorite, but which is less well preserved than the basalt clasts.

The more radiogenic outlying analyses from each of the clasts (those positioned above and left of the basalt clast isochrons) are interpreted as contamination from a KREEP-rich lunar component in the breccia matrix, which occurred during alteration of the basaltic clasts, most likely as a result of an impact. This could also provide a potential source for the radiogenic compositions measured in two of the K-rich glass grains, and would also be consistent with preliminary studies of the meteorite geochemistry indicating that some proportion of the matrix material originated from a more KREEP-rich lithology (Zeigler and Korotev 2016). Furthermore, petrologic evidence of such alteration in the basalt clasts exists in the form of melt veins which cross-cut the other phases in the clasts (Fig. 9a), and post-analysis SEM and EDS mapping imagery of the SIMS spots indicate the presence of small (sub-micron) Zr-rich phases (Fig. 9b-c).

The 4270 ± 10 Ma isochron date determined for the basaltic impact melt Clast 2 is similar to dates obtained for phosphate and baddeleyite grains in the matrix of the meteorite by Shaulis et al. (2016). Although this younger date was interpreted by Shaulis et al. (2016) as the crystallisation age of a younger igneous protolith, the association with an impact melt clast indicates that it may, in fact, represent an impact event. It is not clear if the location of this clast, adjacent to Clast 10, is coincidental or indicates that the impact melt was generated by melting of the same basaltic material, but there is no clear evidence in the Pb isotopic compositions of the two clasts to argue against such a petrogenetic link.

4.2. Initial Pb composition of MIL 13317 basalt

The basalt crystallisation age and best estimate for the initial Pb isotopic composition determined from the clasts in MIL 13317 have been compared with the multiple stage model for the Pb isotopic evolution of lunar silicate reservoirs in the Moon presented by Snape et al. (2016) (Fig. 10). This model was calculated using the measured initial Pb isotopic compositions and ages of several Apollo mare and KREEP basalts, with the assumption that these could be formed from a common source (i.e.

undifferentiated bulk Moon). In the context of this model the bulk Moon evolved from a primitive, Canyon Diablo Troilite (CDT), composition until 4376 ± 18 Ma. At this point, the model indicates that there was a major differentiation event (t_1 in Fig. 10a), resulting in the formation of mantle sources with distinct $^{238}\text{U}/^{204}\text{Pb}$ ratios (μ_2 -values), from which the lunar KREEP and mare basalts were sourced. The timing of this differentiation event is also consistent with Sm-Nd model ages (4360 ± 60 Ma: Lugmair and Carlson 1978; 4320_{-56}^{+40} Ma: Nyquist et al. 1995; 4389 ± 45 Ma: Gaffney and Borg 2014) and Lu-Hf isotopic model ages (4350 - 4430 Ma: Sprung et al. 2013; 4353 ± 37 Ma: Gaffney and Borg 2014; ~ 4340 Ma: McLeod et al. 2014). After 4376 ± 18 Ma, the mantle sources of the mare basalts evolved with μ_2 -values of 360-650, while the sources of the KREEP basalts had μ_2 -values of approximately 2600-3700. This model is inevitably a simplification of lunar mantle differentiation, which almost certainly would not have occurred as a single instantaneous event, with some of the mantle sources forming earlier (such as the mafic cumulates from which the mare basalts originated). As was discussed by Snape et al. (2016), the model differentiation point most likely provides an average approximation for the final stages of LMO crystallisation, including the formation of the anorthositic highland crust and the KREEP-rich reservoir (urKREEP: Warren and Wasson 1979). Despite previous attempts to constrain source μ -values and formation times for the anorthositic crust (e.g. Premo et al. 1999), it is not possible to resolve these different stages of LMO crystallisation in the framework of this model without more unambiguous measurements of initial Pb isotopic compositions for the primary products of these processes (i.e. pristine ferroan anorthosite samples).

The initial Pb isotopic composition determined for the three basaltic clasts in MIL 13317 is consistent with the model growth curves previously predicted for the sources of Apollo basalts (Snape et al. 2016; Fig. 10), and the similarity in time and composition with the predicted differentiation point provides valuable support for the model. Unfortunately, this similarity with the model differentiation composition also means that the μ -value for the source of the basalt clasts cannot be estimated with the same level of precision as those for the basalts in the Snape et al. (2016) study, as the MIL 13317 basalt composition lies at a point in the model where the growth curves for the different reservoirs are very close together. Nonetheless, assuming that the source of the basalts began to evolve from the

model composition at 4376 ± 18 Ma ($^{204}\text{Pb}/^{206}\text{Pb} = 0.036 \pm 0.004$; $^{207}\text{Pb}/^{206}\text{Pb} = 1.59 \pm 0.02$), then it would have evolved with a μ -value of 850 ± 130 (2σ). As such, the source of the MIL 13317 basalts appears to have been more similar to those of relatively KREEP-poor Apollo mare basalts than KREEP-rich samples (including the Apollo 14 high-Al basalt, 14072, and the Apollo 15 KREEP basalt, 15386). This is consistent with mineral chemistries of the pyroxene and plagioclase grains in Clasts 1 and 4 reported by Curran et al. (2016), which were found to be similar to those from VLT and low-Ti Apollo mare basalts.

4.3. Interpretation of Kalahari 009 data

The 4369 ± 7 Ma date determined for the phosphates in Kal 009 is consistent with the previous phosphate U-Pb date of 4350 ± 150 Ma (Terada et al. 2007) and the Lu-Hf date of 4286 ± 95 Ma (Sokol et al. 2008), and slightly older than the Sm-Nd date (4300 ± 50 Ma) determined by Shih et al. (2008). Following the earlier discussion regarding correction of $^{207}\text{Pb}/^{206}\text{Pb}$ ratios (Section 4.1), the case for correcting the Kal 009 phosphate data with a modern day terrestrial Pb model composition is supported by the fact that the phosphate Pb isotopic compositions (including those measured by Terada et al. 2007) and those of the terrestrial weathering products in the sections lie on a regression line, which passes through the Stacey and Kramers (1975) model composition for modern terrestrial Pb. The single phosphate measurement that falls above the regression line (Fig. 8a) is interpreted as containing the highest measured proportion of a lunar initial Pb component, but without more measurements that can be confidently ascribed to this component it is not possible to place any compositional constraint on an initial lunar Pb component.

Terada et al. (2007) interpreted their U-Pb phosphate date as representing the crystallisation age of the Kal 009 basalt. In contrast to this interpretation, the potential for resetting of the U-Pb isotope system in phosphates (Cherniak et al. 1991; Chamberlain and Bowring 2001) has been previously taken advantage of for dating the thermal history of lunar impact breccias (e.g. Nemchin et al. 2009; Thiessen et al. 2017; 2018). The brecciated nature of Kal 009 raises the possibility that the Pb isotopic compositions of the phosphates may be recording an impact event that occurred after the basalt

originally crystallised. Without measurements of phases that are known to be more resistant to resetting of their U-Pb systems (e.g. zircon; Cherniak et al. 1991), it is impossible to be sure from the Pb isotope data alone that the 4369 ± 7 Ma date is indeed an igneous crystallisation age, although it is clear that the VLT basalt sampled by Kal 009 must have erupted by this time. Furthermore, the consistency with the Sm-Nd and Lu-Hf ages provides additional support for this representing the crystallisation age of the basalt.

4.4. Ancient lunar volcanism

These new estimates for the ages of the basaltic material sampled by MIL 13317 and Kal 009, combined with the distinct compositions of this basaltic material (Sokol et al. 2008; Zeigler and Korotev 2016; Curran et al. 2016), support the findings from remote sensing studies of cryptomare deposits (Whitten and Head 2015a), that ancient basaltic volcanism of the Moon produced range of basalt compositions, potentially mirroring that seen in the younger (3800-3000 Ma) mare basalts. Sokol et al. (2008) cited the low-ITE compositions of Kal 009 and its likely pair, Kal 008, as evidence that the meteorites originated from lunar regolith far from the KREEP-rich lithologies of the nearside Procellarum-KREEP Terrane (Jollif et al. 2000). By comparison, the preliminary studies of MIL 13317 indicate that the breccia likely originated from a regolith with a KREEP component (Zeigler and Korotev 2016). Therefore, these meteorites also provide evidence of ancient lunar basaltic volcanism occurring in different regions on the Moon.

The low-ITE abundances in Kal 009 suggest that the basalt parent magma did not assimilate any KREEP-rich material during ascent to the lunar surface. This was previously interpreted as evidence that either the urKREEP reservoir was not present as a global layer around the crust-mantle boundary of the Moon, or that the urKREEP reservoir had not formed prior to the Kal 009 magmatism (Terada et al. 2007). Seeing as the age of Kal 009 (4369 ± 7 Ma) is within error of the Pb model differentiation age (4376 ± 18 Ma; Snape et al. 2016), both of these options remain viable explanations for the low-ITE abundances in the meteorite.

Finally, the occurrence of basaltic volcanism so early in the evolution of the Moon necessitates that there was a mechanism to trigger this magmatic activity almost immediately after LMO crystallisation. Terada et al. (2007) reviewed previous models for lunar basaltic magmatism (Shearer et al. 2006) in relation to Kal 009. They concluded that the low-ITE abundances in the Kal 009 basalt argued against internal heating and melting of the mantle cumulates by radioactive elements present in the source (Wieczorek and Phillips 2000), and that models for large-scale gravitationally driven overturn of the lunar mantle causing mare magmatism several hundred million years after LMO crystallisation (e.g. Hess and Parmentier 1995) were difficult to reconcile with the age of the Kal 009 basalt. This second argument, in particular, is further emphasized by the more precise dating of the meteorite, which places it towards the older end of the age range provided by the previous U-Pb and Lu-Hf studies (Terada et al. 2007; Sokol et al. 2008), and a similar argument can be made regarding the age of the MIL 13317 basalts (4332 ± 2 Ma). Additionally, despite the presence of KREEP-rich material in the regolith that formed the MIL 13317 breccia, the initial Pb isotopic compositions and associated μ -values of the basaltic clasts indicate an absence of significant amounts of ITE- or KREEP-rich material in the sources of the MIL 13317 basaltic components. Having argued against these two mechanisms, Terada et al. (2007) proposed that impact driven melting of the lunar mantle (Elkins-Tanton et al. 2004) provided the most likely mechanism for generating the Kal 009 basaltic magma. If this is the case, then the distinct ages of the basalts identified in these two meteorites suggest that this was not an isolated incident in the Moon's magmatic evolution.

5. Conclusions

The Pb isotopic data presented in this study confirm the ancient ages of basaltic material in the MIL 13317 (4332 ± 2 Ma) and Kal 009 (4369 ± 7 Ma) meteorites (Terada et al. 2007; Sokol et al. 2008; Shaulis et al. 2016). Additionally, the MIL 13317 meteorite provides evidence of an impact event at 4270 ± 10 Ma, based on the age determined for a basaltic impact melt clast. It was also possible to determine an initial Pb isotopic composition for the basalt clasts in MIL 13317, which is consistent with the Pb isotope evolution model of the Moon previously presented by Snape et al. (2016). Based on this initial Pb isotopic composition, the source of the MIL 13317 basalt appears to have evolved

with a μ -value of 850 ± 130 , more consistent with many of the Apollo mare basalts, rather than KREEP-rich lithologies.

The basaltic material in the MIL 13317 and Kal 009 meteorites provides evidence of the earliest known basaltic lunar volcanism. Based on the compositions of the meteorites, this early volcanic activity appears to have generated a range of basalt varieties in different locations on the Moon. These new Pb isotopic data and crystallisation ages are consistent with the hypothesis that large basin forming impacts on the Moon could have led to multiple periods of ancient basaltic magmatism (Elkins-Tanton et al. 2004; Terada et al. 2007).

Acknowledgements

We thank NASA Johnson Space Center for the loan of MIL 13317 and acknowledge the efforts of the ANSMET in collecting the sample. Addi Bischoff is thanked for loaning the polished sections of Kalahari 009. The manuscript benefitted from two anonymous reviews and the editorial handling of Frederic Moynier. This work was primarily funded by grants from the Knut and Alice Wallenberg Foundation (2012.0097) and the Swedish Research Council (VR 621-2012-4370) to MJW and AAN. JFS acknowledges funding from the European Commission Horizon 2020 Research and Innovation programme, through a Marie Skłodowska-Curie Actions Fellowship grant (794287). KHJ acknowledges Royal Society grant RS/UF140190 and STFC grants ST/M001253/1 and ST/R000751/1. NC was funded by an STFC studentship. MA acknowledges funding from Science and Technology Facilities Council (STFC) grants ST/L000776/1 and ST/P000657/1. JJB acknowledges from the Swedish Research Council (VR 2016-03371). At the time of the analytical work, the NordSIMS facility was operated as part of a Swedish-Icelandic infrastructure; this is NordSIMS publication #571. The research has made use of NASA's Astrophysics Data System.

References

- Bellucci J.J., Nemchin A.A., Whitehouse M.J., Snape J.F., Bland P.A. and Benedix G.K. (2015) The Pb isotopic evolution of the Martian mantle constrained by initial Pb in Martian meteorites. *J. Geophys. Res. (Planets)* **120**, 2224–2240. <http://dx.doi.org/10.1002/2015JE004809>
- Chamberlain K. R. and Bowring S. A. (2001) Apatite-feldspar U-Pb thermochronometer: a reliable, mid-range (~450°C), diffusion-controlled system. *Chem. Geology* **172**, 173-200. [http://dx.doi.org/10.1016/S0009-2541\(00\)00242-4](http://dx.doi.org/10.1016/S0009-2541(00)00242-4)
- Cherniak D. J., Lanford W. A. and Ryerson F. J. (1991) Lead diffusion in apatite and zircon using ion implantation and Rutherford Backscattering techniques. *Geochim. Cosmochim. Acta* **55**, 1663-1673. [http://dx.doi.org/10.1016/0016-7037\(91\)90137-T](http://dx.doi.org/10.1016/0016-7037(91)90137-T)
- Curran N. M., Joy K. H., Pernet-Fisher J. F. and Burgess R. (2016) A new basaltic-bearing lunar meteorite Miller Range 13317. 47th Lunar and Planetary Science Conference, abstract no. 1516.
- Curran, N.M., Joy, K.H., Snape, J.F., Pernet-Fisher, J.F., Gilmour, J.D., Nemchin, A.A., Whitehouse, M.J., Burgess, R., (In preparation) The Early Geological History of the Moon Inferred from the Ancient Lunar Meteorite Miller Range 13317. *Meteorit. Planet. Sci.*
- Dasch E. J., Shih C.-Y., Bansal B. M., Wiesmann H. and Nyquist L. E. (1987) Isotopic analysis of basaltic fragments from lunar breccia 14321 - Chronology and petrogenesis of pre-Imbrium mare volcanism. *Geochim. Cosmochim. Acta* **51**, 3241-3254. [http://dx.doi.org/10.1016/0016-7037\(87\)90132-3](http://dx.doi.org/10.1016/0016-7037(87)90132-3)
- Elkins-Tanton L.T., Hager B. H. and Grove T. L. (2004) Magmatic effects of the lunar late heavy bombardment. *Earth Planet. Sci. Lett.* **222**, 17–27. <http://dx.doi.org/10.1016/j.epsl.2004.02.017>
- Gaffney A. M. and Borg L. E. (2014) A young solidification age for the lunar magma ocean. *Geochim. Cosmochim. Acta* **140**, 227–240. <http://dx.doi.org/10.1016/j.gca.2014.05.028>

477 Göpel C., Manhès G. and Allègre C.J. (1985) U-Pb systematics in iron meteorites - Uniformity of
 478 primordial lead. *Geochim. Cosmochim. Acta* **49**, 1681–1695. [http://dx.doi.org/10.1016/0016-](http://dx.doi.org/10.1016/0016-7037(85)90139-5)
 479 [7037\(85\)90139-5](http://dx.doi.org/10.1016/0016-7037(85)90139-5)

480 Head J. W. and Wilson L. (1992) Lunar mare volcanism - Stratigraphy, eruption conditions, and the
 481 evolution of secondary crusts. *Geochim. Cosmochim. Acta* **56**, 2155–2175.
 482 [http://dx.doi.org/10.1016/0016-7037\(92\)90183-J](http://dx.doi.org/10.1016/0016-7037(92)90183-J)

483 Hess P. C. and Parmentier E. M. (1995) A model for the thermal and chemical evolution of the Moon's
 484 interior: implications for the onset of mare volcanism. *Earth Planet. Sci. Lett.* **134**, 501–514.
 485 [http://dx.doi.org/10.1016/0012-821X\(95\)00138-3](http://dx.doi.org/10.1016/0012-821X(95)00138-3)

486 Hiesinger H., Head J. W., Wolf U., Jaumann R. and Neukum G. (2003) Ages and stratigraphy of mare
 487 basalts in Oceanus Procellarum, Mare Nubium, Mare Cognitum, and Mare Insularum. *J.*
 488 *Geophys. Res. (Planets)* **108**, 5065. <http://dx.doi.org/10.1029/2002JE001985>

489 Hiesinger H., Head J. W., Wolf U., Jaumann R. and Neukum G. (2010) Ages and stratigraphy of lunar
 490 mare basalts in Mare Frigoris and other nearside maria based on crater size-frequency distribution
 491 measurements. *J. Geophys. Res. (Planets)* **115**, E03003. <http://dx.doi.org/10.1029/2009JE003380>

492 Jochum, K.P., Nohl, U., Herwig, K., Lammel, E., Stoll, B., Hofmann, A.W., 2005. MPI-DING
 493 glasses: New geological reference materials for in situ Pb isotope analysis. *Geochemistry,*
 494 *Geophysics, Geosystems* **6**, Q10008. <http://dx.doi.org/10.1029/2005GC000995>

495 Jolliff B. L., Gillis J. J., Haskin L. A., Korotev R. L. and Wieczorek M. A. (2000) Major lunar crustal
 496 terranes: Surface expressions and crust-mantle origins. *J. Geophys. Res.* **105**, 4197-4216.
 497 <http://dx.doi.org/10.1029/1999JE001103>

498 Joy K. H. and Arai T. (2013) Lunar meteorites: new insights into the geological history of the Moon.
 499 *Astron. Geophys.* **54**, 4.28-4.32. <http://dx.doi.org/10.1093/astrogeo/att121>

500 Korotev and Irving (2016) Not quite keeping up with the lunar meteorites – 2016. 47th Lunar and
 501 Planetary Science Conference, abstract no. 1358.

502 Kramers J.D. and Tolstikhin I.N. (1997) Two terrestrial lead isotope paradoxes, forward transport
 503 modelling, core formation and the history of the continental crust. *Chem. Geology* **139**, 75–110.
 504 [http://dx.doi.org/10.1016/S0009-2541\(97\)00027-2](http://dx.doi.org/10.1016/S0009-2541(97)00027-2)

505 Ludwig K. R. (2008) User's Manual for Isoplot 3.60, A geochronological toolkit for Microsoft Excel.
 506 *Berkeley Geochronological Center Special Publication* **4**, Berkeley, California: Berkeley
 507 Geochronological Center.

508 Lugmair G.W. and Carlson R.W. (1978) The Sm-Nd history of KREEP. *Lunar Planet. Sci. IX*. Lunar
 509 Planet. Inst., Houston. pp. 689-704.

510 McLeod C.L., Brandon A.D. and Armitage R.M.G. (2014) Constraints on the formation age and
 511 evolution of the Moon from ^{142}Nd - ^{143}Nd systematics of Apollo 12 basalts. *Earth Planet. Sci. Lett.*
 512 **396**, 179–189. <http://dx.doi.org/10.1016/j.epsl.2014.04.007>

513 Neal C. R. and Taylor L. A. (1992) Petrogenesis of mare basalts – A record of lunar volcanism.
 514 *Geochim. Cosmochim. Acta* **56**, 2177-2211. [http://dx.doi.org/10.1016/0016-7037\(92\)90184-K](http://dx.doi.org/10.1016/0016-7037(92)90184-K)

515 Neal C. R. and Kramer G. Y. (2006) The petrogenesis of the Apollo 14 high-Al mare basalts. *Am.*
 516 *Mineral.* **91**, 1521-1535. <http://dx.doi.org/10.2138/am.2006.2147>

517 Nemchin A. A., Pidgeon R. T., Healy D., Grange M. L., Whitehouse M. J. and Vaughan J. (2009) The
 518 comparative behavior of apatite-zircon U-Pb systems in Apollo 14 breccias: Implications for the
 519 thermal history of the Fra Mauro Formation. *Meteorit. Planet. Sci.* **44**, 1717-1734.
 520 <http://dx.doi.org/10.1111/j.1945-5100.2009.tb01202.x>

521 Nemchin A. A., Jeon H., Bellucci J. J., Timms N. E., Snape J. F., Kilburn M. R. and Whitehouse M. J.
 522 (2017) Pb-Pb ages of feldspathic clasts in two Apollo 14 breccia samples. *Geochim. Cosmochim.*
 523 *Acta* **217**, 441-461. <http://dx.doi.org/10.1016/j.gca.2017.08.024>

524 Nyquist L.E. and Shih C.-Y. (1992) The isotopic record of lunar volcanism. *Geochim. Cosmochim.*
 525 *Acta* **56**, 2213–2234. [http://dx.doi.org/10.1016/0016-7037\(92\)90185-L](http://dx.doi.org/10.1016/0016-7037(92)90185-L)

526 Nyquist L.E., Wiesmann H., Bansal B., Shih C.-Y., Keith J.E. and Harper C.L. (1995) ^{146}Sm - ^{142}Nd
527 formation interval for the lunar mantle. *Geochim. Cosmochim. Acta* **59**, 2817-2837.
528 [http://dx.doi.org/10.1016/0016-7037\(95\)00175-Y](http://dx.doi.org/10.1016/0016-7037(95)00175-Y)

529 Premo W. R., Tatsumoto M., Misawa K., Nakamura N. and Kita N. I. (1999) Pb-Isotopic Systematics
530 of Lunar Highland Rocks (>3.9 Ga): Constraints on Early Lunar Evolution. *Int. Geol. Rev.* **41**,
531 95-128. <http://dx.doi.org/10.1080/00206819909465134>

532 Russell S. S., Zolensky M., Righter K., Folco L., Jones R., Connolly H. C., Grady M. M. and
533 Grossman J. N. (2005) The Meteoritical Bulletin, No. 89, 2005 September. *Meteorit. Planet. Sci.*
534 **40**, Supp. A201-A263.

535 Satterwhite C. and Righter K. (2015) *Antarctic Meteorite Newsletter*, **38**, No. 2.

536 Schultz P. H. and Spudis P. D. (1979) Evidence for ancient lunar mare volcanism. *Lunar Planet. Sci.*
537 **X**. Lunar Planet. Inst., Houston. pp. 2899-2918.

538 Schultz P. H. and Spudis P. D. (1983) Beginning and end of lunar mare volcanism. *Nature* **302**, 233-
539 236. <http://dx.doi.org/10.1038/302233a0>

540 Shaulis B. J., Kring D. A., Lapen T. J., and Righter M. (2016) Petrology and distribution of U-Pb ages
541 in lunar meteorite breccia Miller Range (MIL) 13317. 47th Lunar and Planetary Science
542 Conference, abstract no. 2033.

543 Shearer C. K., Hess P. C., Wiczorek M. A., Pritchard M. E., Parmentier E. M., Borg L. E., Longhi J.,
544 Elkins-Tanton L. T., Neal C. R., Antonenko I., Canup R. M., Halliday A. N., Grove T. L., Hager
545 B. H., Lee D. C. and Wiechert U. (2006) Thermal and magmatic evolution of the Moon. *Rev.*
546 *Mineral. Geochem.* **60**, 365-518. <http://dx.doi.org/10.2138/rmg.2006.60.4>

547 Shih C.-Y., Nyquist L. E., Bogard D. D., Bansal B. M., Wiesmann H., Johnson P., Shervais J. W. and
548 Taylor L. A. (1986) Geochronology and Petrogenesis of Apollo 14 Very High Potassium Mare
549 Basalts. *Lunar Planet. Sci. XVI*. Lunar Planet. Inst., Houston. pp. 214-228.

550 Shih C.-Y., Nyquist L. E., Bogard D. D., Dasch E. J., Bansal B. M. and Wiesmann H. (1987)
 551 Geochronology of high-K aluminous mare basalt clasts from Apollo 14 breccia 14304. *Geochim.*
 552 *Cosmochim. Acta* **51**, 3255–3271. [http://dx.doi.org/10.1016/0016-7037\(87\)90133-5](http://dx.doi.org/10.1016/0016-7037(87)90133-5)

553 Shih C.-Y., Nyquist L. E., Reese Y, and Bischoff A. (2008) Sm-Nd and Rb-Sr isotopic studies of
 554 meteorite Kalahari 009: An old VLT mare basalt. 39th Lunar and Planetary Science Conference,
 555 abstract no. 2165.

556 Shimizu N. and Hart S. R. (1982) Isotope fractionation in secondary ion mass spectrometry. *Journal of*
 557 *Applied Phys.* **53**, 1303-1311. <http://dx.doi.org/10.1063/1.330636>

558 Snape J. F., Nemchin A. A., Bellucci J. J., Whitehouse M. J., Tartèse R., Barnes J. J., Anand M.,
 559 Crawford I. A. and Joy K. H. (2016) Lunar basalt chronology, mantle differentiation and
 560 implications for determining the age of the Moon. *Earth Planet. Sci. Lett.* **451**, 149-158.
 561 <http://dx.doi.org/10.1016/j.epsl.2016.07.026>

562 Snape J. F., Nemchin A. A., Bellucci J. J. and Whitehouse M. J. (2017) Pb isotopes in the impact melt
 563 breccia 66095: Association with the Imbrium basin and the isotopic composition of lithologies at
 564 the Apollo 16 landing site. *Chem. Geol.* **466**, 608-616.
 565 <http://dx.doi.org/10.1016/j.chemgeo.2017.07.012>

566 Snape J. F., Davids D., Nemchin A. A., Whitehouse M. J. and Bellucci J. J. (2018) Constraining the
 567 timing and sources of volcanism at the Apollo 12 landing site using new Pb isotopic compositions
 568 and crystallisation ages. *Chem. Geol.* **482**, 101-112.
 569 <http://dx.doi.org/10.1016/j.chemgeo.2018.02.009>

570 Sokol A. K., Fernandes V. A., Schulz T., Bischoff A., Burgess R., Clayton R. N., Münker C.,
 571 Nishiizumi K., Palme H., Schultz L., Weckwerth G., Mezger K. and Horstmann M. (2008)
 572 Geochemistry, petrology and ages of the lunar meteorites Kalahari 008 and 009: New constraints
 573 on early lunar evolution. *Geochim. Cosmochim. Acta* **72**, 4845–4873.
 574 <http://dx.doi.org/10.1016/j.gca.2008.07.012>

575 Sprung P., Kleine T. and Scherer E. E. (2013) Isotopic evidence for chondritic Lu/Hf and Sm/Nd of
 576 the Moon. *Earth Planet. Sci. Lett.* **380**, 77-87. <http://dx.doi.org/10.1016/j.epsl.2013.08.018>

577 Stacey J. S. and Kramers J. D. (1975) Approximation of terrestrial lead isotope evolution by a two-
 578 stage model. *Earth Planet. Sci. Lett.* **26**, 207-221. [http://dx.doi.org/10.1016/0012-](http://dx.doi.org/10.1016/0012-821X(75)90088-6)
 579 [821X\(75\)90088-6](http://dx.doi.org/10.1016/0012-821X(75)90088-6)

580 Taylor L. A., Shervais J. W., Hunter R. H., Shih C. -Y., Bansal B. M., Wooden J., Nyquist L. E. and
 581 Laul L. C. (1983) Pre-4.2 AE mare-basalt volcanism in the lunar highlands. *Earth Planet. Sci.*
 582 *Lett.* **66**, 33-47. [http://dx.doi.org/10.1016/0012-821X\(83\)90124-3](http://dx.doi.org/10.1016/0012-821X(83)90124-3)

583 Terada K. and Sano Y. (2003) In situ U-Pb dating and REE analyses of phosphates in extraterrestrial
 584 materials. *Applied Surface Science* **203-204**, 810-813. [http://dx.doi.org/10.1016/S0169-](http://dx.doi.org/10.1016/S0169-4332(02)00831-0)
 585 [4332\(02\)00831-0](http://dx.doi.org/10.1016/S0169-4332(02)00831-0)

586 Terada K., Anand M., Sokol A. K., Bischoff A. and Sano Y. (2007) Cryptomare magmatism 4.35 Gyr
 587 ago recorded in lunar meteorite Kalahari 009. *Nature* **450**, 849-852.
 588 <http://dx.doi.org/10.1038/nature06356>

589 Thiessen F., Nemchin A. A., Snape J. F., Whitehouse M. J. and Bellucci J. J. (2017) Impact history of
 590 the Apollo 17 landing site revealed by U-Pb SIMS ages. *Meteorit. Planet. Sci.* **52**, 584-611.
 591 <http://dx.doi.org/10.1111/maps.12814>

592 Thiessen F., Nemchin A. A., Snape J. F., Bellucci J. J. and Whitehouse M. J. (2018) Apollo 12
 593 breccia 12013: Impact-induced partial Pb loss in zircon and its implications for lunar
 594 geochronology. *Geochim. Cosmochim. Acta* **230**, 94-111.
 595 <http://dx.doi.org/10.1016/j.gca.2018.03.023>

596 Warren P. H. and Wasson J. T. (1979) The origin of KREEP. *Rev. Geophys. Space Phys.* **17**, 73-88.
 597 <http://dx.doi.org/10.1029/RG017i001p00073>

598 Wieczorek M. A. and Phillips R. J. (2000) The "Procellarum KREEP Terrane": Implications for mare
 599 volcanism and lunar evolution. *J. Geophys. Res.* **105**, 20417–20430.
 600 <http://dx.doi.org/10.1029/1999JE001092>

601 Whitehouse M. J., Kamber B. S., Fedo C. M. and Lepland A. (2005) Integrated Pb- and S-isotope
 602 investigation of sulphide minerals from the early Archaean of southwest Greenland. *Chem. Geol.*
 603 **222**, 112-131. <http://dx.doi.org/10.1016/j.chemgeo.2005.06.004>

604 Whitten J. and Head J. W. (2015a) Lunar cryptomaria: Mineralogy and composition of ancient
 605 volcanic deposits. *Planet. Space Sci.* **106**, 67-81. <http://dx.doi.org/10.1016/j.pss.2014.11.027>

606 Whitten J. L. and Head J. W. (2015b) Lunar cryptomaria: Physical characteristics, distribution, and
 607 implications for ancient volcanism. *Icarus* **247**, 150-171.
 608 <http://dx.doi.org/10.1016/j.icarus.2014.09.031>

609 Woodhead J. D. and Hergt J. M. (2000) Pb-Isotope Analyses of USGS Reference Materials. *Geostand.*
 610 *Geoanal. Res.* **24**, 33-38. <http://dx.doi.org/10.1111/j.1751-908X.2000.tb00584.x>.

611 Zartman R. E. and Doe B. R. (1981) Plumbotectonics – The model. *Tectonophysics* **75**, 135-162.
 612 [http://dx.doi.org/10.1016/0040-1951\(81\)90213-4](http://dx.doi.org/10.1016/0040-1951(81)90213-4)

613 Zeigler R. A. and Korotev R. L. (2016) Petrography and geochemistry of lunar meteorite Miller Range
 614 13317. 47th Lunar and Planetary Science Conference, abstract no. 2554.

Figures

Figure 1. – (a) Back Scattered Electron (BSE) image of the MIL 13317,7 thin section with the clasts analysed in this study annotated. More detailed images of the individual clasts are provided in panels (b-e). Plag – plagioclase; Pyx – pyroxene; Sil – silica.

Figure 2. – Back Scattered Electron (BSE) images of typical textures in the Kal 009 meteorite. The dashed line in panel (a) indicates the approximate boundary between an area of more well preserved igneous texture and the more common brecciated texture in the meteorite, where the phosphates analysed in this study were located. The effects of terrestrial weathering and contamination are apparent in veins and fractures throughout the sample, which are commonly filled with either Ca-rich material (BSE image and corresponding Ca X-ray element map in panels (b-c)) or K-rich material (BSE image and corresponding K X-ray element map in panels (d-e)). Note, the brightest areas in the BSE images are the remnants of gold coating from previous SIMS analyses present in cracks and divots in the sections. Plag – plagioclase; Pyx – pyroxene; Oliv – olivine; Symp – symplectite.

Figure 3. – $^{207}\text{Pb}/^{206}\text{Pb}$ vs. $^{204}\text{Pb}/^{206}\text{Pb}$ plots of the complete datasets from (a) the four basaltic clasts and (b) the impact melt clast in MIL 13317. The grey triangles represent the predicted range of compositions that would result from three-component mixing between the initial Pb isotopic compositions of the rocks, the more radiogenic Pb generated by the decay of U after the rocks formed and a terrestrial contaminant (represented here with the model composition of modern terrestrial Pb presented by Stacey and Kramers 1975; “S+K”). Analyses (plotted in partially transparent symbols) lying to the right of sample isochron (i.e. the left side of the triangle) and within this mixing triangle are filtered out as containing significant amounts of terrestrial contamination.

Figure 4. – $^{207}\text{Pb}/^{206}\text{Pb}$ vs. $^{204}\text{Pb}/^{206}\text{Pb}$ plots of the filtered data sets for the MIL 13317 basalt clasts (a-e). A combined isochron and initial Pb isotopic composition was generated for the four basaltic clasts with ages of ~4330 Ma (f). Error bars represent 2σ uncertainties and uncertainties for the isochron dates are stated at the 95% confidence level.

640 Figure 5. – (a) $^{207}\text{Pb}/^{206}\text{Pb}$ vs. $^{204}\text{Pb}/^{206}\text{Pb}$ plot of data from the MIL 13317 matrix grains. An expanded
641 plot of the most radiogenic compositions is shown in panel (b). Error bars represent 2σ uncertainties.
642 The combined isochron for the four ~4330 Ma basaltic clasts in the sample (see Fig. 3) has also been
643 indicated for comparison with the matrix grain compositions. The matrix phosphate, baddeleyite and
644 zircon data are from Curran et al. (in review). Error bars represent 2σ uncertainties.

645 Figure 6. – $^{208}\text{Pb}/^{206}\text{Pb}$ vs. $^{204}\text{Pb}/^{206}\text{Pb}$ plots of the filtered data sets for the five MIL 13317 basalt
646 clasts. Grey triangular fields mark the range of compositions in each sample. Error bars represent 2σ
647 uncertainties.

648 Figure 7. – $^{207}\text{Pb}/^{206}\text{Pb}$ ages for phosphate grains in Kal 009. The ages were calculated from $^{207}\text{Pb}/^{206}\text{Pb}$
649 ratios corrected for the presence terrestrial Pb, using the model composition of Stacey and Kramers
650 (1975). Box heights represent 2σ uncertainties.

651 Figure 8. – (a) $^{204}\text{Pb}/^{206}\text{Pb}$ vs. $^{207}\text{Pb}/^{206}\text{Pb}$ plot of data from Kal 009. A regression through the majority
652 of the analyses equates to an age of 4369 ± 7 Ma (95% conf.), while a single outlying phosphate
653 analysis (partially transparent symbol) would lie within a mixing triangle between the initial Pb
654 composition of the basalt, the radiogenic Pb from decay of U after the basalt crystallised and a
655 terrestrial contaminant. (b) The data collected in this study have been compared with the Stacey and
656 Kramers (1975) model composition for modern day terrestrial Pb (S+K) and the phosphate analyses
657 previously made by Terada et al. (2007). Error bars represent 2σ uncertainties. Note that, despite
658 falling on the regression line through the sample data points, the Stacey and Kramers (1975) model
659 value was not included in the calculation of this line, but its inclusion in this plot demonstrates why
660 equivalent age estimates for Kal 009 are obtained from both this regression and the weighted average
661 of the terrestrial common Pb corrected phosphate $^{207}\text{Pb}/^{206}\text{Pb}$ ages

662 Figure 9. – (a) BSE image of the Clast 1 boundary (dashed white line) with breccia matrix in MIL
663 13317. Vein originating from the matrix and penetrating into the clast is indicated with white arrows.
664 (b) BSE image showing the location of SIMS spot (dashed white ellipse) in Clast 4 of MIL 13317,
665 which provided radiogenic outlier K-rich glass composition. A BSE-bright fleck of Zr-rich material

was identified in the SIMS target area, in addition to a number of other compositional heterogeneities and a nearby vein, which are apparent in the element maps of the area (c-e).

Figure 10. – (a) Schematic chart outlining the multi-stage Pb isotopic evolution model of Snape et al. (2016), the solid arrows indicate the stages represented in the model calculations. (b) Initial Pb isotopic composition of the MIL 13317 basalt clasts compared with the model of Snape et al. (2016). The model is calculated assuming lunar formation at 4500 Ma and a primitive starting composition of Canyon Diablo Troilite (CDT; Göpel et al. 1985). In the model, an undifferentiated bulk Moon with a μ_1 -value of ~ 460 evolves until 4376 ± 18 Ma. The mantle sources of the main Apollo basaltic suites can all be modelled as originated from the model differentiation composition with distinct μ_2 -values. The initial Pb isotopic compositions of the Apollo 11 high-Ti basalt 10044, Apollo 12 low-Ti basalts 12038, 12039 and 12063, the KREEP-rich Apollo 14 high-Al basalts 14072 and the KREEP basalt 15386 have also been plotted for comparison (data originally presented in Snape et al. 2016). (c) Focusing just on the region between the model differentiation point at 4376 ± 18 Ma and the MIL 13317 basalts, the μ_2 -value (920 ± 350 ; 2σ) necessary to form this composition within the model framework, would have been more similar to that attributed to the Apollo mare basalt sources than that of the high- μ KREEP basalt sources. Error bars and the Pb growth curve fields represent 2σ uncertainties.

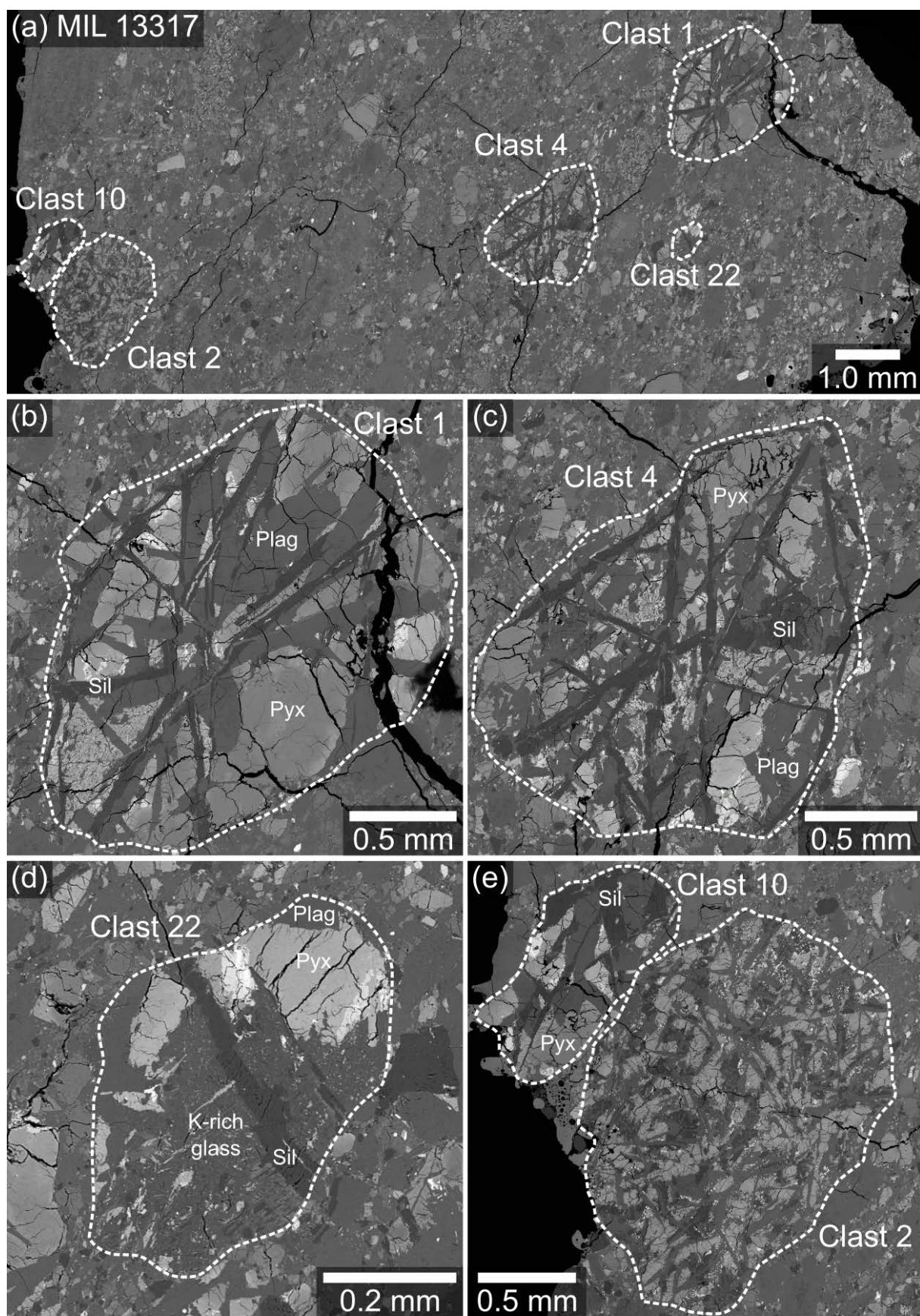


Figure 1

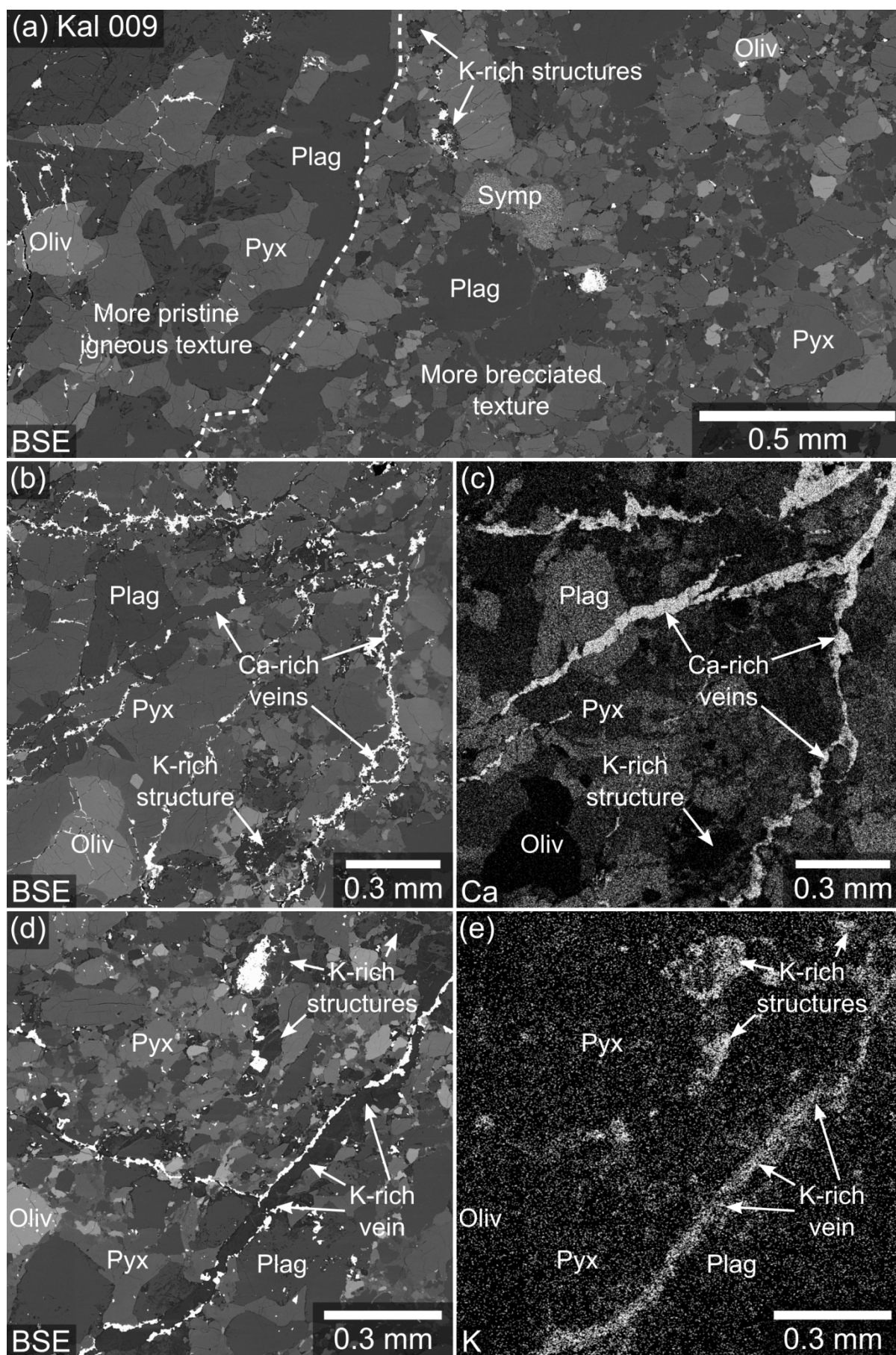


Figure 2

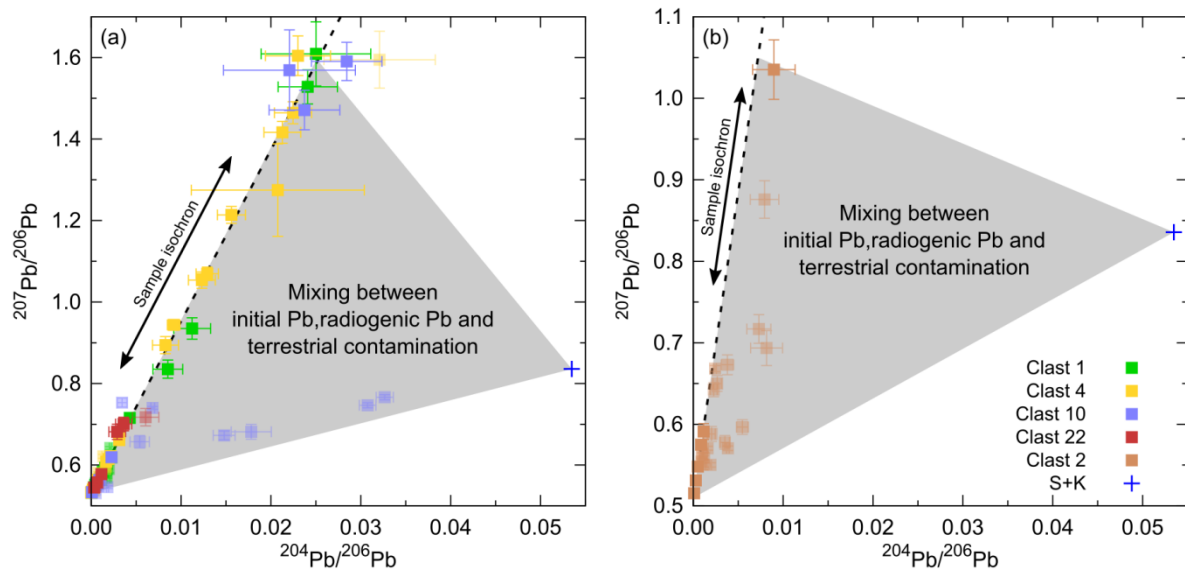


Figure 3

685

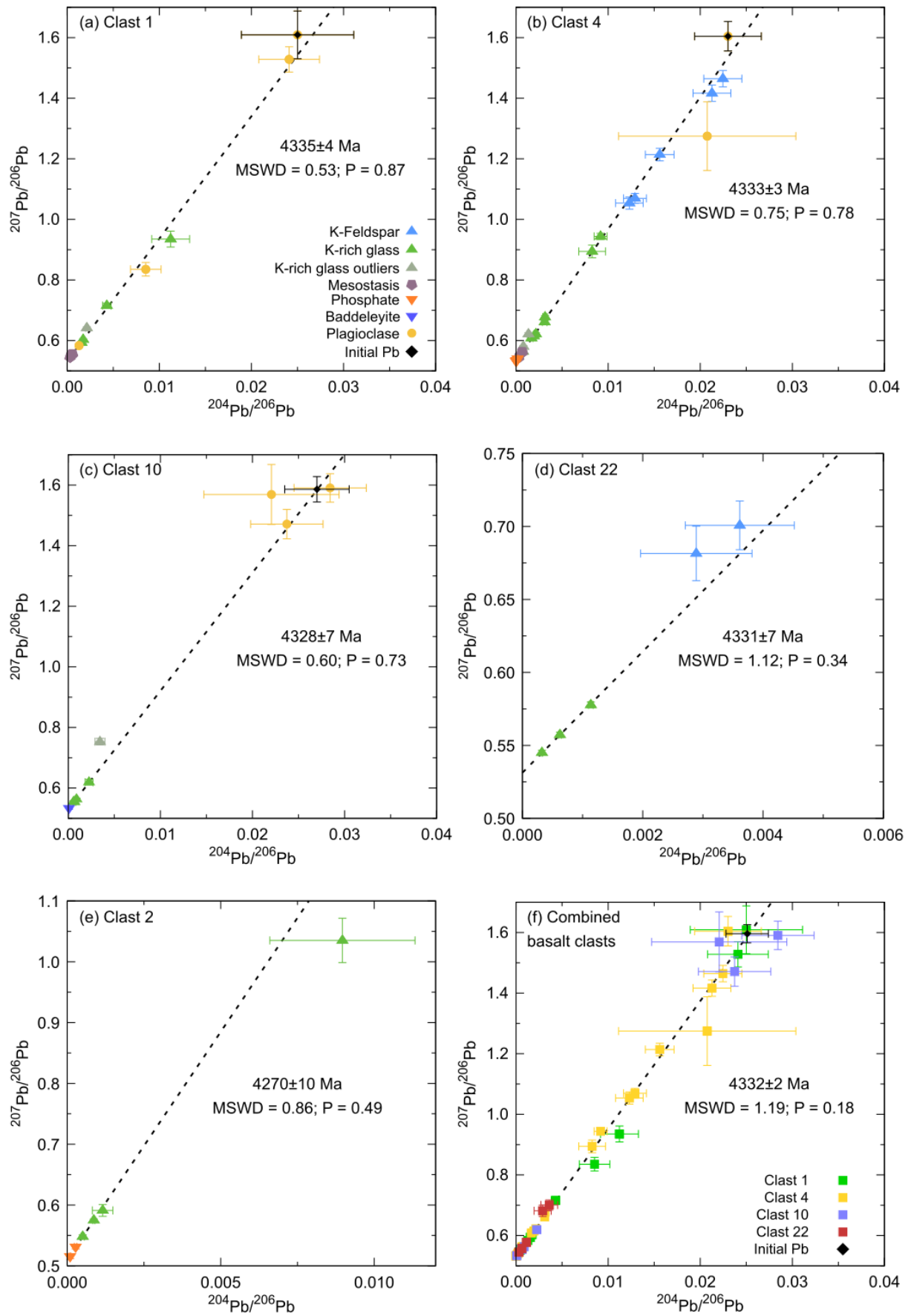


Figure 4

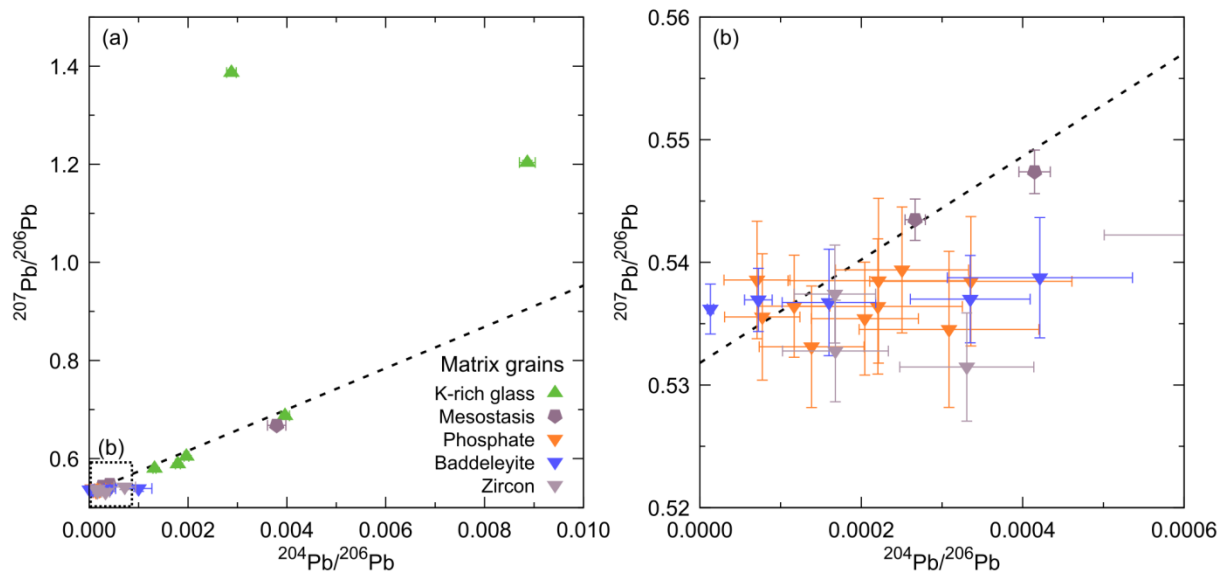
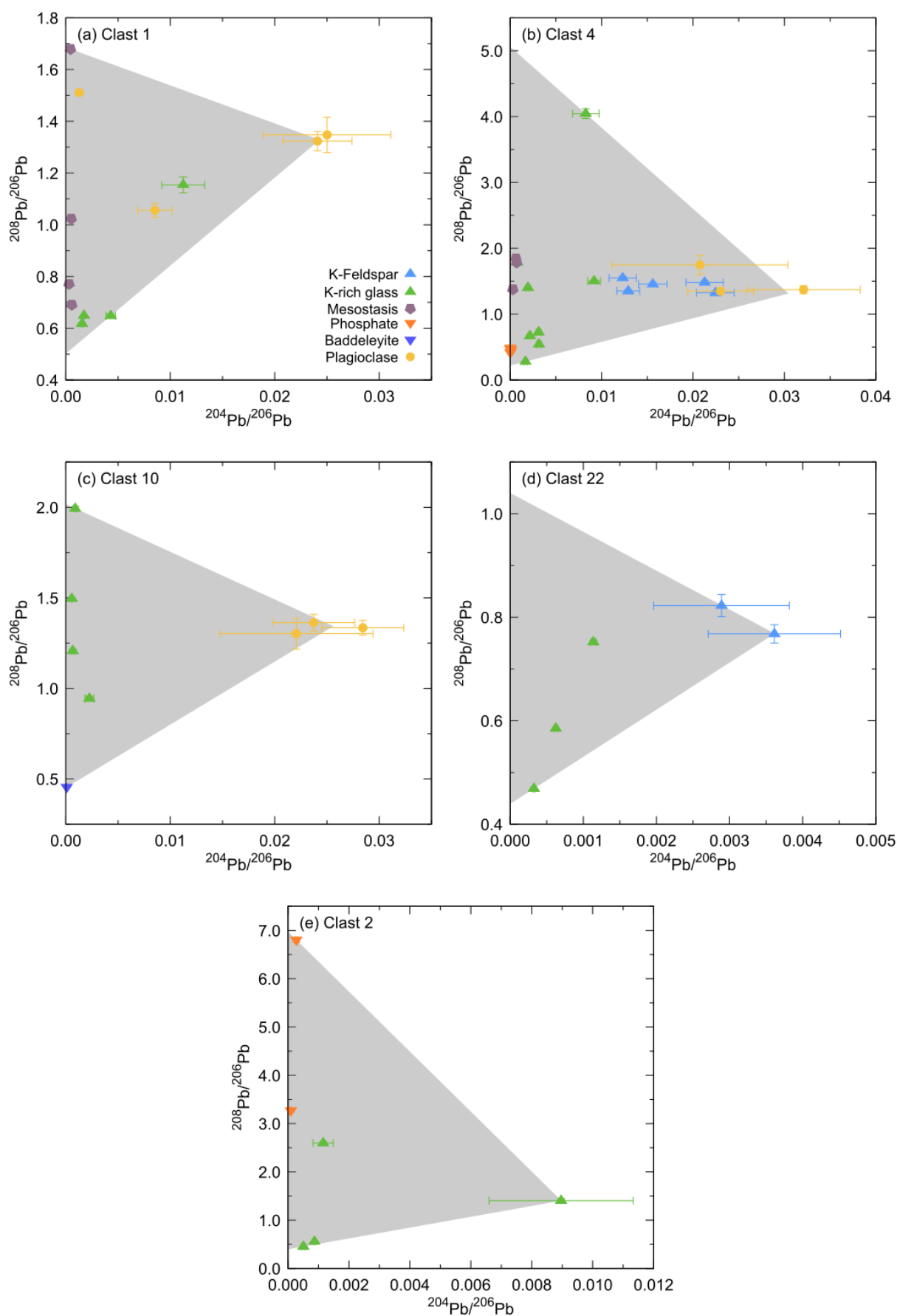


Figure 5



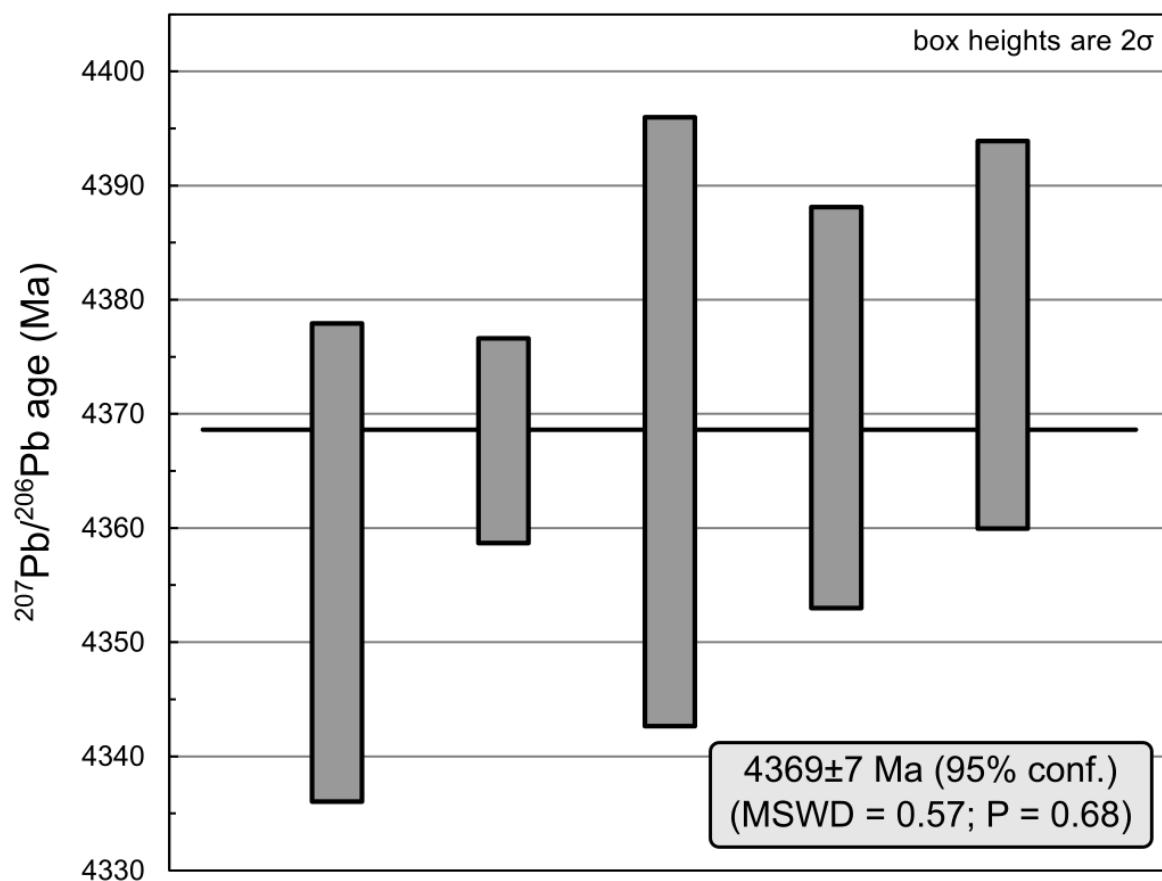


Figure 7

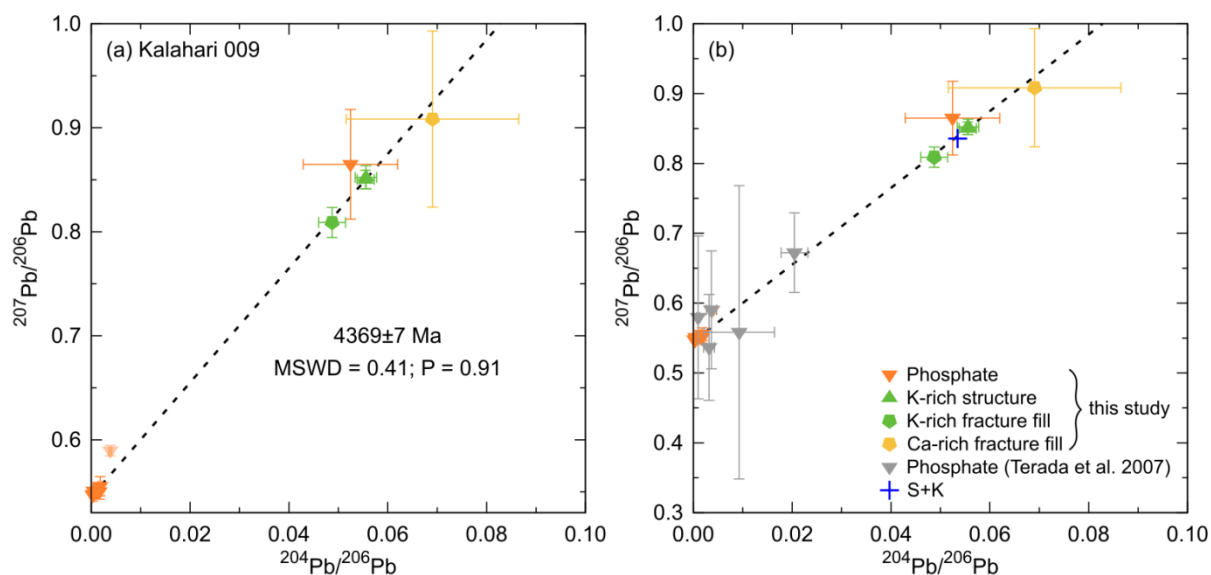


Figure 8

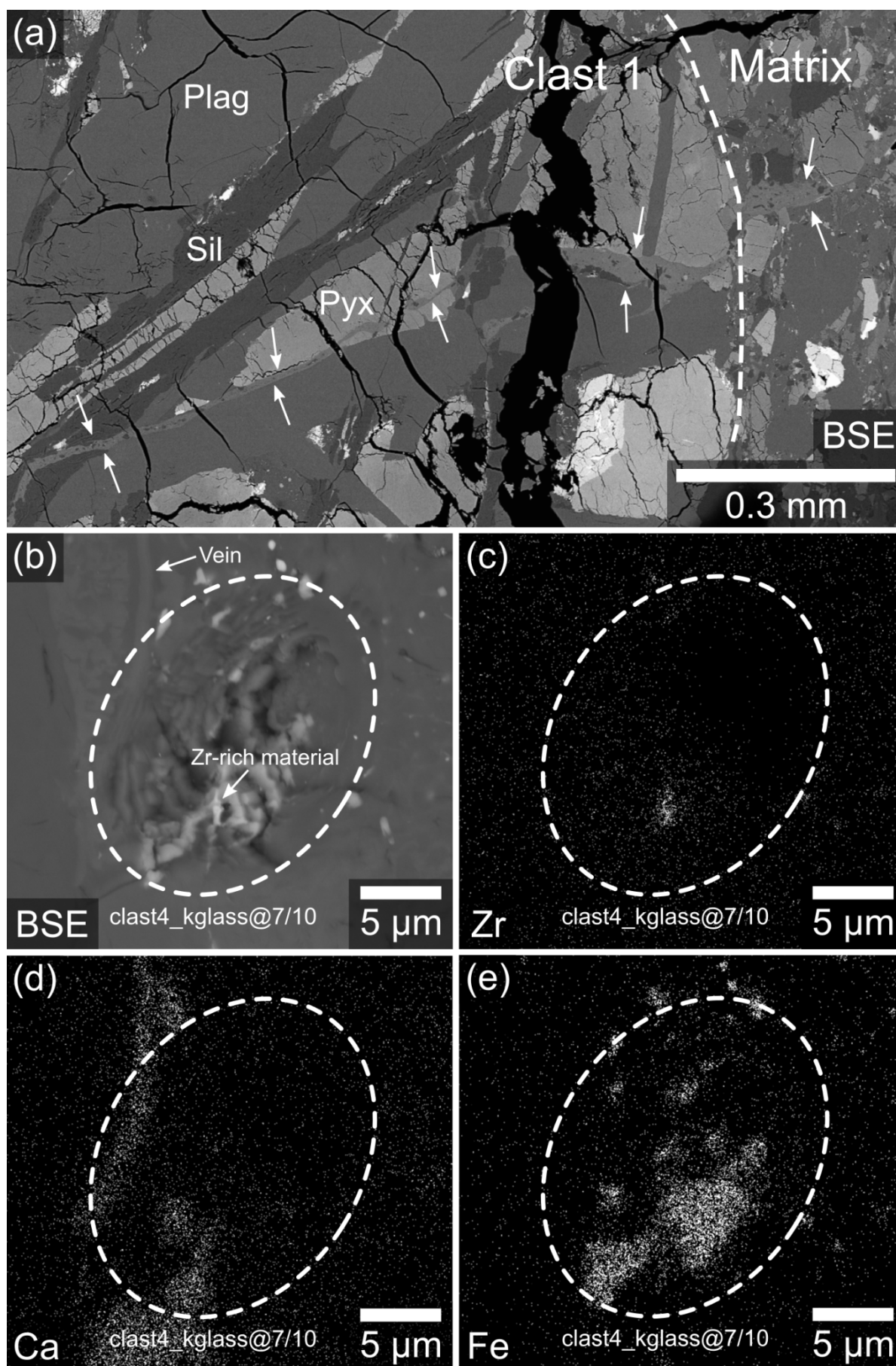


Figure 9

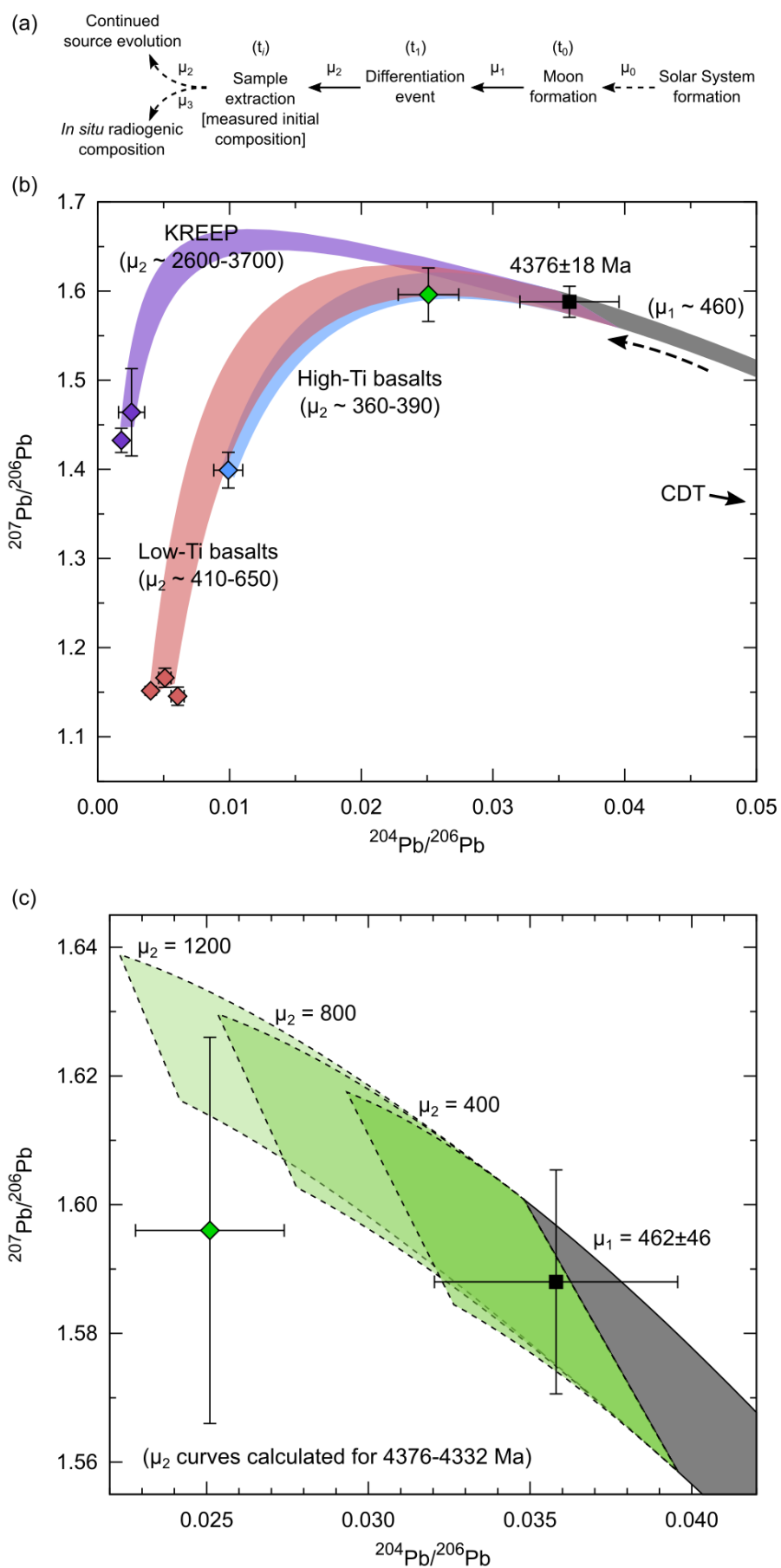


Figure 10

	$^{207}\text{Pb}/^{206}\text{Pb}$ isochron date (Ma)	\pm	MSWD	Probability of fit	$^{204}\text{Pb}/^{206}\text{Pb}$	$\pm 2\sigma$	$^{207}\text{Pb}/^{206}\text{Pb}$	$\pm 2\sigma$	$^{208}\text{Pb}/^{206}\text{Pb}$	$\pm 2\sigma$
Clast 1	4335	4	0.53	0.87	0.025	0.006	1.61	0.08	1.35	0.07
Clast 4	4333	3	0.75	0.78	0.027	0.004	1.59	0.04	1.33	0.04
Clast 10	4328	7	0.60	0.73	0.025	0.003	1.60	0.04	1.36	0.04
Clast 22	4331	7	1.12	0.34			Not determined			
Clast 2	4270	10	0.86	0.49			Not determined			
Combined basaltic clasts	4332	2	1.19	0.18	0.025	0.002	1.60	0.03	1.34	0.03

693

694 Table 1 – Summary of the $^{207}\text{Pb}/^{206}\text{Pb}$ isochron dates determined for each of the basalt clasts in MIL 13317, as well as the combined isochron for the basalt
695 clasts (Clasts 1, 4, 10 and 22). Also included are the best estimates for the initial Pb isotopic composition of the clasts, where it was possible to determine one.
696 Uncertainties for the isochron dates are stated at the 95% confidence level.

Supplementary material

Appendix A – Supplementary Figures

Figure A.1. – Back Scattered Electron (BSE) maps of the MIL 13317,7 (a) and the Kal 009 (b-c) thin sections analysed in this study.

Figure A.2. – Pyroxene compositions of Kal 009 (Sokol et al. 2008) compared with those of Apollo 12 (Boyd and Smith 1971; Dence et al. 1971; Weill et al. 1971; Hollister et al. 1971; Keil et al. 1971; Shearer et al. 1989; Alexander et al. 2014) and 15 (Walker et al. 1977) low-Ti basalts, as well as those in VLT gabbro MIL 05035 (Joy et al. (2008).

Figure A.3. – Plagioclase compositions of Kal 009 (Sokol et al. 2008) compared with those of Apollo 12 low-Ti basalts (Taylor et al. 1971; Keil et al. 1971; Crawford et al. 1973; Alexander et al. 2014) and VLT gabbro MIL 05035 (Joy et al. (2008).

Figure A.4. – Complete datasets from the MIL 13317 clasts plotted to show the data that were filtered out to generate the isochrons for each clast.

Figure A.5. – Alternative isochron (black dashed line) for the basaltic clasts in MIL 13317 incorporating the outlier compositions described in the main text. Note that the resulting isochron date (4330 ± 3 Ma; MSWD = 1.05; P = 0.4) is within error of the combined basalt clast isochron presented in the main text (indicated here by the grey dashed line), primarily due to the very low $^{204}\text{Pb}/^{206}\text{Pb}$ ratios of the most radiogenic analyses (i.e. those with the lowest $^{204}\text{Pb}/^{206}\text{Pb}$ and $^{207}\text{Pb}/^{206}\text{Pb}$ ratios). An expanded plot of the most radiogenic analyses has been included in panel (b) for extra clarity.

Appendix B – Supplementary Tables

Table B.1. – Complete SIMS datasets.

Table B.2. – Average electron multiplier background levels for each analytical session.

Table B.3. – Average measured values of the GOR 132-G and BCR-2G reference materials during each analytical session.